The RFI 2022 Workshop at ECMWF, 14 – 18 February 2022
2022 URSI International Union of Radio Science

RFI Mitigation via Auto-Encoder Framework in SAR Data

Jiang Liu(1), Yunxuan Wang(1), Yuan Mao(1), Junli Chen(2), Yanyang Liu(2), and Yan Huang*(1)
(1) State Key Lab of Millimeter Waves, Southeast University, Jiangsu, China
(2) Shanghai Institute of Satellite Engineering, Shanghai, China

Abstract

With the increasing demand for better range resolution for synthetic aperture radar (SAR), radio frequency interference (RFI) blocking SAR imaging becomes a major issue in accurate remote sensing by a SAR system, which greatly affects the SAR imaging and the following interpretation process. We proposed a SAR interference suppression method based on an automatic encoder to tackle the problem. An automatic encoder-based RFI mitigation network (RMN) is built and trained based on the SAR signal polluted by the narrowband interference and the wideband interference. The input of the RMN is time-frequency diagrams contaminated with interferences, useful information about the target signal is extracted through the self-encoder network structure, and the original time-frequency diagram of the target echo signal is reconstructed by the network. The proposed method's ability to automatically suppress the narrowband and wideband interference is demonstrated through numerical experiments.

Index Terms—Synthetic aperture radar (SAR), radio-frequency interference (RFI) mitigation, auto-encoder

1 Introduction

With the development of electronics and mobile wireless technology, radio devices have an increasing demand for greater bandwidth. The radar system also requires larger bandwidth to obtain better range resolution, especially for imaging radar systems represented by synthetic aperture radar (SAR). Hence, radio frequency interference (RFI) becomes a major issue in accurate remote sensing by a SAR system, which greatly affects the SAR imaging and the following interpretation process.

During the past decades, many researchers working on how to effectively mitigate RFIs from collected SAR data. These methods can be approximately classified into three categories, i.e., non-parametric methods, parametric methods, and semi-parametric methods [1]. Non-parametric methods mainly employ filters to filter out interference or project the original data onto a signal subspace [2, 3]. Parametric methods commonly estimate the parameters of RFIs, including the narrowband and wideband models [4]. Semi-parametric methods use the machine learning models, such as sparse encoder [5] and low-rank recovery methods [6, 7, 8], to mitigate RFIs from measured data.

Recently, deep learning tools have excellent performance for nearly all the tasks in computer vision and natural language processing areas. For the supervised learning frameworks, they can extract the hierarchical features of targets in the images and further be employed to classify different targets. Previous methods, such as the deep convolutional neural network (D-CNN), were used to mitigate both the narrowband and wideband interferences in SAR images [9]. For the unsupervised learning frameworks, i.e., auto-encoder [10] and generative adversarial network (GAN) [11], they can discover intrinsic properties of the data without any pre-assigned labels and are widely leveraged in the image denoising area. Also, the PCA-based unsupervised learning methods [12] are widely used to mitigate RFIs in corrupted SAR data. Therefore, we come out with the idea that unsupervised learning frameworks have great potential to separate the RFI and the useful data. In this paper, we use an auto-encoder framework, combining real and imaginary parts of complex radar data as two branches, to mitigate strong RFIs from corrupted SAR data. It brings another perspective to RFI mitigation via a deep unsupervised learning approach.

2 Signal Model

In SAR systems, the received signal at range time t and azimuth time τ can be modeled as

$$x(t,\tau) = s(t,\tau) + I(t,\tau) + n(t,\tau), \tag{1}$$

where $s(t,\tau)$, $I(t,\tau)$,and $n(t,\tau)$ denote the target received signal, RFI, and additive noise, respectively. These RFIs can be classified into two categories, i.e., the narrowband interference (NBI) and the wideband interference (WBI). NBI can be expressed as

$$I_{\mathrm{NB}}(t,\tau) = \sum_{k=1}^{K} a_k(t,\tau) \exp j(2\pi f_k t + \phi_k), \tag{2}$$

where $a_k(t,\tau)$, f_k, and ϕ_k denote the complex amplitude, frequency ,and initial phase of the kth interference, respectively. The WBI commonly have two forms, i.e., the chirp-modulated (CM) WBI and the sinusoidal-modulated (SM)

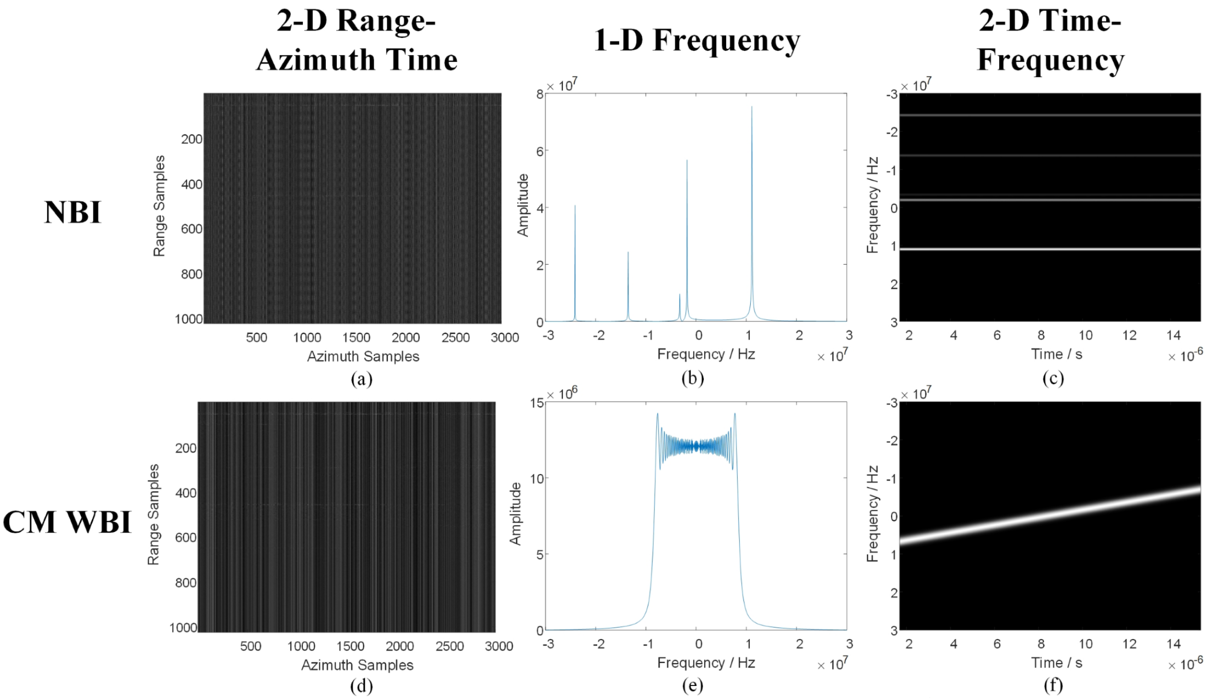

Figure 1. The characteristics of interference in the different domain. (a) Narrowband interference in the 2D range-azimuth time domain. (b) Narrowband interference in the 1D frequency domain. (c) Narrowband interference in the 2D time frequency domain. (d) Chirp-modulated wideband interference in the 2D range-azimuth time domain. (e) Chirp-modulated wideband interference in the 1D frequency domain. (f) Chirp-modulated wideband interference in the 2D time frequency domain.

WBI. The CM WBI is more typical for RFIs and can be formulated as

$$I_{\mathrm{CM}}(t,\tau)=\sum_{k=1}^{K}a_k(t,\tau)\exp j(2\pi f_k t+\pi\gamma_k t^2), \tag{3}$$

where $a_k(t,\tau)$, f_k, and γ_k denote the complex amplitude, frequency, and modulation frequency of the k-th interference, respectively. Before analyzing the properties of NBI and WBI, we first introduce the short-time Fourier transform (STFT) to transform the signal vector into time-frequency domain. The basic idea of STFT is to perform Fourier transform (FT) to a certain part of the signal vector $y(t)$ via a smoothing window $h(t)$. Then the STFT can be formulated as

$$\mathrm{STFT}_y(t,f)=\int_{-\infty}^{+\infty}y(t)h(t-\tau)e^{-j2\pi f\tau}\mathrm{d}\tau, \tag{4}$$

where (t,f) indicates the coefficient in the time-frequency domain. Similarly, the inverse STFT (ISTFT) is performed with the synthesis window $w(t)$ as

$$y(t)=\int_{-\infty}^{+\infty}\int_{-\infty}^{+\infty}\mathrm{STFT}_y(t',f')w(t-t')e^{j2\pi f't'}\mathrm{d}t'\mathrm{d}f'. \tag{5}$$

Then the characteristics of both NBI and CM WBI in the 2-D time domain, 1-D frequency domain, and 2-D time-frequency domain are shown in Figure. 1. The NBI performs like several strips in the 2-D time-frequency domain, and the CM WBI looks like a slant line, showing linear frequency modulation property. But both RFIs perform irregularly in the 2-D time domain and it is hard to recognize any interpretative objects. This inspires us to mitigate the RFIs in the 2-D time-frequency domain.

3 Proposed Auto-Encoder Method

In this section, we will introduce an RFI mitigation method based on the auto-encoder network with its specific layers.

Table 1. Structure of the Interference Mitigation Auto-Encoder Networks

Layer	Radar Echo Time-Frequency Diagram
1	separable_conv2d (3,3,64), stride=1, ReLU
2	batch_normalization
3	separable_conv2d (3,3,64), stride=1, ReLU
4	batch_normalization
5	separable_conv2d (3,3,128), stride=1, ReLU
6	batch_normalization
7	separable_conv2d (3,3,128), stride=1, ReLU
8	batch_normalization
9	separable_conv2d (3,3,128), stride=1, ReLU
10	batch_normalization
11	separable_conv2d (3,3,128), stride=1, ReLU
12	batch_normalization
13	separable_conv2d (3,3,64), stride=1, ReLU
14	batch_normalization
15	separable_conv2d (3,3,64), stride=1, ReLU
16	batch_normalization
17	separable_conv2d (3,3,1), stride=1

As analyzed before, the RFIs have distinctive features in the time-frequency domain. Therefore, it is easy to remove RFIs in this domain rather than the image domain. The DCNN can extract features, textures, and other useful information in SAR images. For the RFIs mitigation problem, we propose an RFI mitigation network (RMN) to mitigate strong RFIs, exploiting the advantages of deep learning methods. Previous works usually leverage a supervised learning network, but the proposed RMN is based on the auto-encoder, one of the most typical unsupervised-learning networks. The inputs of the RMN are the time-frequency diagram of the RFI-polluted signals and the expected outputs of the RMN are the time-frequency diagram of the RFI-free signals. The encoder extracts useful features and the decoder is used to recover the RFI-free signal. The RMN uses nine depth-wise separable convolutional (DSC) layers [13] and eight batch normalization layers. The size of the convolutional kernel is 3 by 3, and the stride is 1. The specific layers are listed in Table 1.

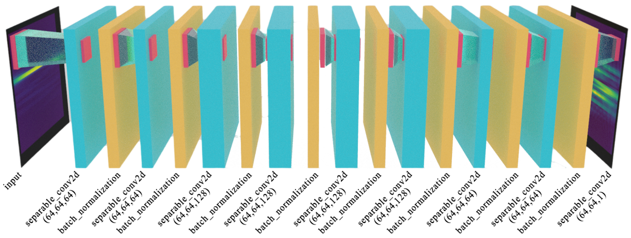

Figure 2. Structure of the interference mitigation auto-encoder networks.

The DSC layers we applied in the network can be regarded as a variant of a traditional convolutional layer. As we can see from Figure. 3 (a), the traditional convolution layer takes the convolution of the whole data with one kernel, which has the same depth as the data. If we suppose that the input size of the data is $M \times M \times N$ and the kernel size is $K \times K \times N \times P$. Then the parameter number of the traditional convolutional layer can be simply calculated as $K \times K \times N \times P$, without considering the bias number. However, different from the traditional convolutional layer, the DSC layer has two convolutions. As can be seen in Figure. 3 (b), we first take the convolution of each data channel with each kernel channel, so the output depth is N. Then the P dot product or the $1 \times 1 \times N \times P$ kernel is used to finish the other convolution. The total parameter number of the DSC layer is $(K \times K \times N + N \times P)$, which is much smaller than the total parameter number of the traditional convolutional layer. Therefore, with the same number of parameters, the networks with DSC layers can go deeper than the networks with traditional convolutional layers.

The loss function used in the network is defined by mean square error (MSE), which can be expressed as

$$L_{\mathrm{MSE}}^{\mathrm{RMN}} = \frac{1}{MN} \sum_{m=1}^{M} \sum_{n=1}^{N} [I_{\mathrm{ori}}(m,n) - G_{\mathrm{RMN}}(I_{\mathrm{input}}(m,n))]^2, \tag{6}$$

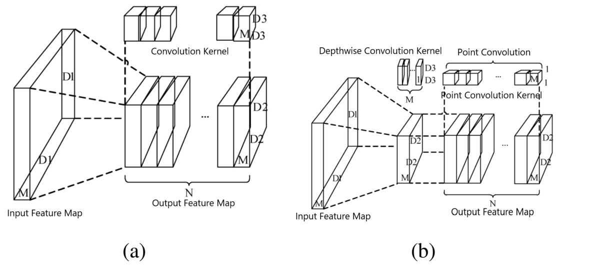

Figure 3. (a) Schematic diagram of standard convolutional layer. (b) Schematic diagram of Depth-wise separable convolutional layer.

where the input size of the time-frequency diagram is $M \times N$. Herein, I_{ori} and I_{input} are the RFI-free and RFI-polluted time-frequency diagrams, respectively. G_{RMN} denotes the network output. In this paper, we divide the whole time-frequency diagram into many parts with their size being 64 by 64. The time-frequency diagrams are constructed by complex data and we normalize the whole data and separate it into the real parts and imaginary parts. Then the input data size is $64 \times 64 \times 2$ and the whole network is listed in Table 1. The batch is set to 20 and the learning rate is 0.001. We use RMSProp as the optimization method and Glorot as the initialization method.

4 Experimental Results

In this section, we use the collected SAR data contaminated with simulated RFIs to provide enough data and support the RMN training. Two indexes are used to quantitatively evaluate the performance of the proposed RMN, i.e., interference suppression ratio (ISR) [14] and signal distortion ratio (SDR) [15]. The two indexes are expressed as,

$$\mathrm{ISR} = 10\log_{10}\left(\frac{\sum |x|^2}{\sum |\hat{x}|^2}\right), \tag{7}$$

$$\mathrm{SDR} = 10\log_{10}\left(\frac{\sum |x_0 - \hat{x}|^2}{\sum |x_0|^2}\right), \tag{8}$$

where x_0, x and $\hat{x}$ denote the RFI-free, RFI-polluted, and RFI-removal results, respectively. The larger the ISR and the smaller the SDR indicates better RFI mitigation performance.

Herein, we consider two scenarios, one is contaminated by the narrowband RFI and the other one is contaminated by the wideband RFI. The input signal-to-interference-and-noise ratio (SINR) is -20 dB. We illustrate the time-frequency diagrams of the narrowband RFI-polluted data and the RFI-free data in Figure. 4 (a) and (c). As we can see from the time-frequency diagrams, the interference is so strong that the RFI-free signal is submerged by the interferences. The imaging result of the RFI-contaminated SAR signals is shown in Figure. 4 (d), and the RFI-free SAR image is shown in Figure. 4 (f). We apply the proposed RMN to remove the narrowband RFI, the results are shown

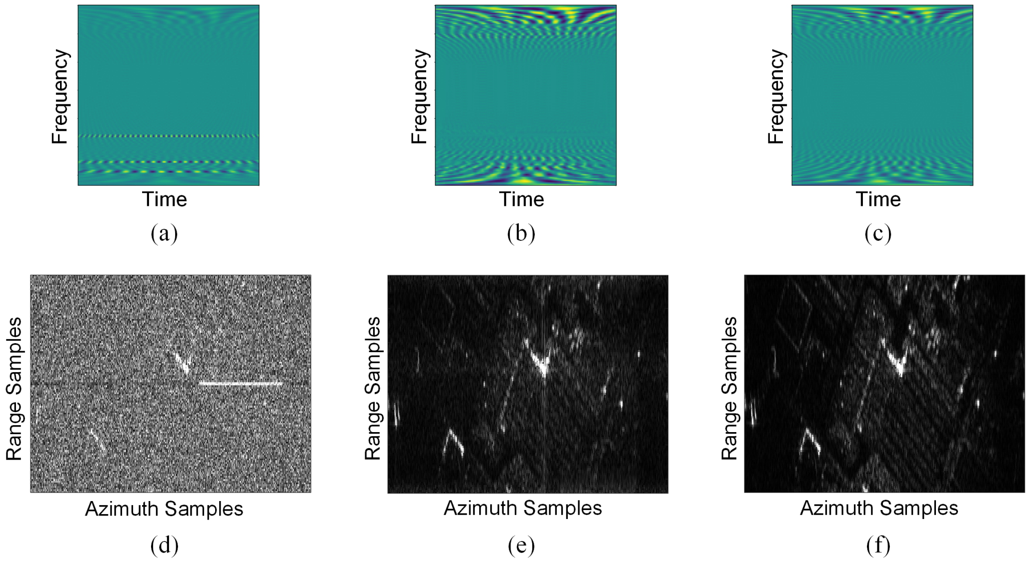

Figure 4. (a) The time-frequency diagram of narrowband-interference-contaminated SAR echo signal. (b) The time-frequency diagram of narrowband-interference-mitigated SAR echo signal via RMN method. (c) The time-frequency diagram of no interference-contaminated SAR echo signal. (d) The SAR image of narrowband-interference-contaminated SAR echo signal. (e) The SAR image of narrowband-interference-mitigated SAR echo signal via RMN method. (f) The SAR image of no interference-contaminated SAR echo signal.

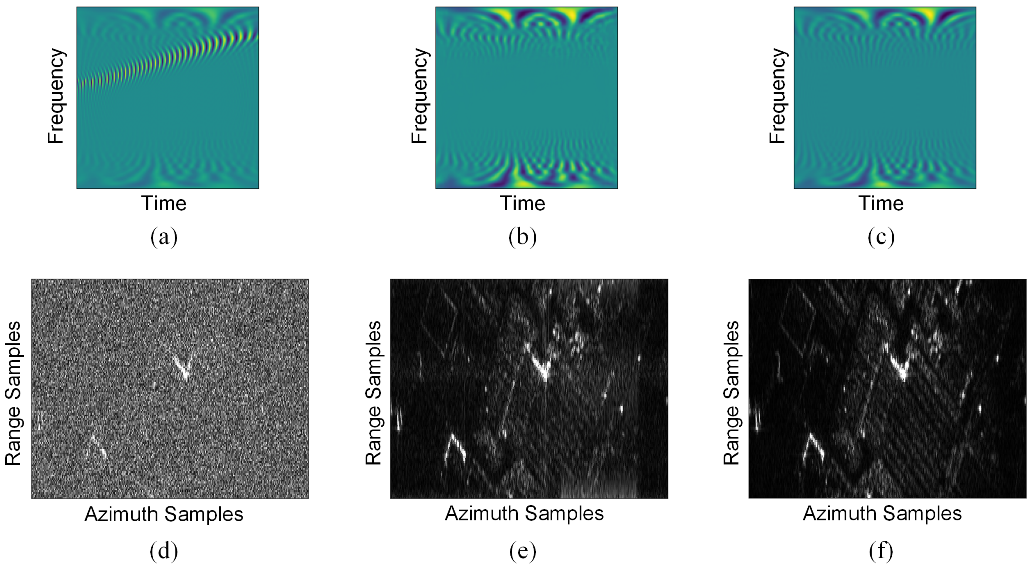

Figure 5. (a) The time-frequency diagram of wideband-interference-contaminated SAR echo signal. (b) The time-frequency diagram of wideband-interference-mitigated SAR echo signal via RMN method. (c) The time-frequency diagram of no interference-contaminated SAR echo signal. (d) The SAR image of wideband-interference-contaminated SAR echo signal. (e) The SAR image of wideband-interference-mitigated SAR echo signal via RMN method. (f) The SAR image of no interference-contaminated SAR echo signal.

in Figure. 4 (b) and (e). The recovered result is quite similar to the RFI-free one. The ISR is 5.33 dB and the SDR is -12.34 dB, which indicates the good performance of interference mitigation.

Next, we demonstrate the proposed RMN on the CM wideband RFI case. The RFI-polluted and RFI-free time-frequency diagrams are shown in Figure. 5 (a) and (c). Due to the strong power of RFI, the RFI also dominates the whole diagram with only a few useful signals can be seen. The imaging diagram of the RFI contaminated SAR signals is shown in Figure. 5 (d), the RFI-free SAR image is shown in Figure. 5 (f). The recovered result is shown in Figure. 5 (b). For this case, the ISR is 5.50 dB and the SDR is -12.79 dB. The imaging result after the RMN processing is shown in Figure. 5 (e). As the two numerical experiments show, the proposed RMN has acceptable performance for strong RFI mitigation, including the narrowband and wideband RFIs.

5 Conclusion

This work presented narrowband and wideband RFI occurred in SAR systems and explored their time-frequency characteristics. We proposed a SAR interference mitigation method based on auto-encoder, which takes the time-frequency diagram of the interference contaminated SAR signal as the input, and reconstructs recovered SAR signal as the output. We used MSE as the loss function of the network and applied depth-wise separable convolution layers to accelerate the model learning as well as to improve the stability of the network. We demonstrated the feasibility of our methods by numerical simulations.

6 Acknowledgements

This work was supported in part by the National Natural Science Foundation of China under Grant 61901112, in part by the Natural Science Foundation of Jiangsu Province under Grant BK20190330, and in part by Shanghai Aerospace Science and Technology Innovation Fund under Grant SAST2021-043.

References

[1] Y. Huang, B. Zhao, M. Tao, et.al. “Review of synthetic aperture radar interference suppression,” *Journal of Radars*, 2020, 9(1): 86–106. doi: 10.12000/JR19113.

[2] F. Zhou, R. Wu, M. Xing, and Z. Bao, “Eigensubspace-based filtering with application in narrow-band interference suppression for SAR,” *IEEE Geosci. Remote Sens. Lett.,* vol. 4, no. 1, pp. 75-79, 2007.

[3] R. Lord, “Radio frequency interference suppression applied to synthetic aperture radar data,” *XXVIIIth General Assembly of International Union of Radio Science,* URSI, New Delhi, India, Oct. 2005.

[4] Z. Liu, G. Liao, and Z. Yang, “Time variant RFI suppression for SAR using iterative adaptive approach,” *IEEE Geosci. Remote Sens. Lett.,* vol. 10, no. 6, pp. 1424-1428, 2013.

[5] H. Liu, D. Li, Y. Zhou, and T. Truong, “Simultaneous radio frequency and wideband interference suppression in SAR signals via sparsity exploitation in time-frequency domain,” *IEEE Trans. Geosci. Remote Sens.*, vol. 56, no. 10, pp. 5780-5793, 2018.

[6] Y. Huang, L. Zhang, X. Yang, Z. Chen, J. Liu, J. Li, and W. Hong, “An efficient graph-based algorithm for time-varying narrowband interference suppression on SAR system,” *IEEE Trans. Geosci. Remote Sens.*, vol. 59, no. 10, 2021, DOI: 10.1109/TGRS.2021.3051192.

[7] Y. Huang, L. Zhang, J. Li, Z. Chen, and X. Yang, “Reweighted tensor factorization method for SAR narrowband and wideband interference mitigation using smoothing multiview tensor model,” *IEEE Trans. Geosci. Remote Sens.*, vol. 58, no. 5, pp. 3298-3313, 2020.

[8] Y. Huang, Z. Chen, C. Wen, J. Li, X. Xia, W. Hong, “An Efficient Radio Frequency Interference Mitigation Algorithm in Real Synthetic Aperture Radar Data,” *IEEE Trans. Geosci. Remote Sens.*, vol. 60, 2022, DOI: 10.1109/TGRS.2022.3155068.

[9] W. Fan, F. Zhou, M. Tao, X. Bai, P. Rong, S. Yang, T. Tian, “Interference Mitigation for Synthetic Aperture Radar Based on Deep Residual Network,” *Remote Sensing*, **11**(14), 2019, 1654, doi: 10.3390/rs11141654.

[10] Y. Wang, H. Yao, S. Zhao, “Auto-encoder based dimensionality reduction,” *Neurocomputing*, **184**, 2016, pp. 232–242, doi: 10.1016/j.neucom.2015.08.104.

[11] I. Goodfellow, J. Pouget-Abadie, M. Mirza, B. Xu, D. Warde-Farley, S. Ozair, A. Courville, Y. Bengio, “Generative Adversarial Nets,” *Advances in Neural Information Processing Systems*, **27**, 2014.

[12] M. Tao, J. Su, Y. Huang, L. Wang. “Mitigation of Radio Frequency Interference in Synthetic Aperture Radar Data: Current Status and Future Trends. Remote Sensing,” **11**(20), 2019, 2438, doi: 10.3390/rs11202438

[13] F. Chollet, “Xception: Deep Learning with Depthwise Separable Convolutions,” *2017 IEEE Conference on Computer Vision and Pattern Recognition (CVPR)*, Honolulu, HI, 2017, pp. 1800-1807, doi: 10.1109/CVPR.2017.195.

[14] M. Tao, F. Zhou and Z. Zhang, “Wideband Interference Mitigation in High-Resolution Airborne Synthetic Aperture Radar Data,” *IEEE Transactions on Geoscience and Remote Sensing*, **54**, Jan. 2016, pp. 74–87, doi: 10.1109/TGRS.2015.2450754.

[15] F. Zhou and M. Tao, "Research on Methods for Narrow-Band Interference Suppression in Synthetic Aperture Radar Data," *IEEE Journal of Selected Topics in Applied Earth Observations and Remote Sensing*, **8**, July 2015, pp. 3476-3485, doi: 10.1109/JSTARS.2015.2431916.